PLOS | COMPUTATIONAL BIOLOGY

RESEARCH ARTICLE

Spatial separation of two different pathways accounting for the generation of calcium signals in astrocytes

Franziska Oschmann[1,2¤]*, Konstantin Mergenthaler[1], Evelyn Jungnickel[1], Klaus Obermayer[1,2¤]

1 Technische Universität Berlin, Neural Information Processing Group, Berlin, Germany, **2** Bernstein Center for Computational Neuroscience, Berlin, Germany

¤ Current address: Technische Universität Berlin, Neural Information Processing Group, Berlin, Germany
* oschmann@ni.tu-berlin.de

Citation: Oschmann F, Mergenthaler K, Jungnickel E, Obermayer K (2017) Spatial separation of two different pathways accounting for the generation of calcium signals in astrocytes. PLoS Comput Biol 13(2): e1005377. doi:10.1371/journal.pcbi.1005377

Editor: Jeffrey J. Saucerman, University of Virginia, UNITED STATES

Received: September 1, 2016

Accepted: January 23, 2017

Published: February 13, 2017

Data Availability Statement: All relevant data are within the paper and its Supporting Information files.

Funding: This work was supported by Bundesministerium für Bildung und Forschung: 01GQ 1009 (KM) https://www.bmbf.de/ and Deutsche Forschungsgemeinschaft, Graduiertenkolleg 1589 http://www.dfg.de/. The funders had no role in study design, data collection and analysis, decision to publish, or preparation of the manuscript.

Abstract

Astrocytes integrate and process synaptic information and exhibit calcium (Ca^{2+}) signals in response to incoming information from neighboring synapses. The generation of Ca^{2+} signals is mostly attributed to Ca^{2+} release from internal Ca^{2+} stores evoked by an elevated metabotropic glutamate receptor (mGluR) activity. Different experimental results associated the generation of Ca^{2+} signals to the activity of the glutamate transporter (GluT). The GluT itself does not influence the intracellular Ca^{2+} concentration, but it indirectly activates Ca^{2+} entry over the membrane. A closer look into Ca^{2+} signaling in different astrocytic compartments revealed a spatial separation of those two pathways. Ca^{2+} signals in the soma are mainly generated by Ca^{2+} release from internal Ca^{2+} stores (mGluR-dependent pathway). In astrocytic compartments close to the synapse most Ca^{2+} signals are evoked by Ca^{2+} entry over the plasma membrane (GluT-dependent pathway). This assumption is supported by the finding, that the volume ratio between the internal Ca^{2+} store and the intracellular space decreases from the soma towards the synapse. We extended a model for mGluR-dependent Ca^{2+} signals in astrocytes with the GluT-dependent pathway. Additionally, we included the volume ratio between the internal Ca^{2+} store and the intracellular compartment into the model in order to analyze Ca^{2+} signals either in the soma or close to the synapse. Our model results confirm the spatial separation of the mGluR- and GluT-dependent pathways along the astrocytic process. The model allows to study the binary Ca^{2+} response during a block of either of both pathways. Moreover, the model contributes to a better understanding of the impact of channel densities on the interaction of both pathways and on the Ca^{2+} signal.

Author summary

Astrocytes are considered as active partners in neural information processing, because they integrate and process synaptic information and control synaptic transmission. Neuronal transmitter release induces the generation of Ca^{2+} signals in astrocytes. The

Competing interests: The authors have declared that no competing interests exist.

functional role of astrocytic Ca^{2+} signals is still under debate. However, experimental results were able to show that astrocytic Ca^{2+} signaling acts to control local network activity, which plays an important role in diseases like epilepsy. Thus, it is of special interest to investigate the underlying mechanisms for Ca^{2+} signals in astrocytes in order to understand the role of astrocytes in neural network activity. Two different mechanisms are known to be responsible for the generation of Ca^{2+} signals in astrocytes. These mechanisms are the release of Ca^{2+} from internal Ca^{2+} stores and the entry of Ca^{2+} through the plasma membrane. We studied the interaction of those two different mechanisms for the generation of Ca^{2+} signals and found that these mechanisms are spatially separated along the astrocytic processes.

Introduction

Astrocytes integrate and process synaptic information and by doing so generate calcium (Ca^{2+}) signals in response to neurotransmitter release from neighboring synapses [1]. Ca^{2+} signals in astrocytes are largely attributed to an elevated metabotropic glutamate receptor (mGluR) activity, which stimulates the phospholipase C and the production of the second messenger inositol trisphosphate (IP_3). The binding of IP_3 to receptors at internal Ca^{2+} stores (endoplasmatic reticulum) induces IP_3 and Ca^{2+}-dependent Ca^{2+} release into the intracellular space [2–7] (see mGluR-dependent pathway in Fig 1).

Experimental results, however, showed not only a clear attenuation of the Ca^{2+} signal during an inhibition of the mGluR, but also during a block of the glutamate transporter (GluT) [7, 8]. The glutamate transporter itself does not influence the intracellular Ca^{2+} concentration, but it indirectly activates Ca^{2+} entry over the membrane mediated by the Na^+/Ca^{2+} exchanger [9] (see GluT-dependent pathway in Fig 1). The uptake of one glutamate molecule mediated by the glutamate transporter is accompanied by the transport of three sodium (Na^+) ions into the astrocyte and one potassium (K^+) ion out of the astrocyte. An inwardly directed Na^+ gradient and an outwardly directed K^+ gradient promote the glutamate uptake by the glutamate transporter and glutamate accumulation in the astrocyte. The Na^+-K^+-ATPase maintains the Na^+-K^+ concentration gradient and favors the glutamate transport [10]. In close proximity to glutamate transporters high concentrations of Na^+/Ca^{2+} exchangers have been observed [9]. During a rapid rise of the Na^+ concentration the Na^+/Ca^{2+} exchanger works in the reverse mode and transports Na^+ out of the astrocyte while transporting Ca^{2+} into the astrocyte. Thereby the Na^+/Ca^{2+} exchanger serves as an additional transient source of Ca^{2+} and the intracellular Ca^{2+} concentration increases [9].

Therefore, at least two different mechanisms contribute to the generation of Ca^{2+} signals in astrocytes. A closer look into Ca^{2+} signaling in different astrocytic compartments revealed a spatial separation of those two pathways. In the soma Ca^{2+} signals are mainly evoked on the mGluR-dependent pathway, whereas in perisynaptic astrocytic processes (PAPs) most Ca^{2+} signals are evoked by Ca^{2+} entry over the plasma membrane [11]. These results are supported by the finding, that astrocytic compartments close to the synapse are devoid of internal Ca^{2+} stores and the volume ratio of internal Ca^{2+} stores compared to the intracellular space increases towards the soma. Moreover, the surface volume ratio decreases along the astrocytic process from the PAPs towards the soma, because processes become increasingly thinner (see Fig 2) [12].

Based on the findings cited above we hypothesized that the underlying mechanisms for Ca^{2+} signals differ between astrocytic compartments. The mGluR-dependent pathway is

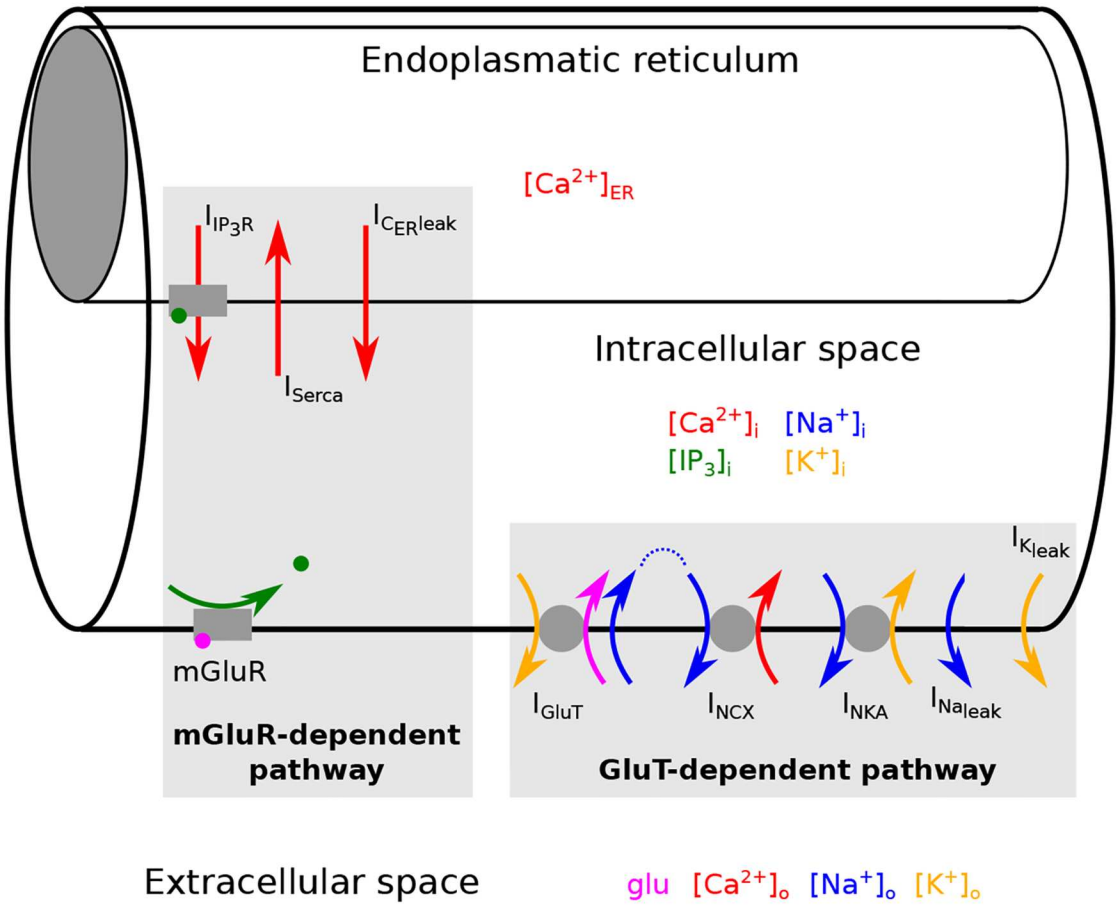

Fig 1. Generation of Ca^{2+} signals in an astrocyte. We consider astrocytic compartments which consist of three parts: the intracellular space, the internal Ca^{2+} store (endoplasmatic reticulum) and the extracellular space. Ca^{2+} signals in the intracellular space are generated by two different pathways: the metabotropic glutamate receptor (mGluR)-dependent pathway and the glutamate transporter (GluT)-dependent pathway. The mGluR-dependent pathway describes the glutamate dependent production of IP_3, which then evokes IP_3 and Ca^{2+} dependent exchange of Ca^{2+} between the intracellular space and the endoplasmatic reticulum. The GluT-dependent pathway describes the GluT driven transport of Ca^{2+} between the extracellular and the intracellular space.

doi:10.1371/journal.pcbi.1005377.g001

mainly present close to the astrocytic soma, while the GluT-dependent pathway dominates Ca^{2+} signals in PAPs. So far most mathematical models attribute astrocytic Ca^{2+} dynamics solely to mGluRs and neglect Ca^{2+} entry through the membrane. In order to test whether the Na^+/Ca^{2+} exchanger serves as a source for Ca^{2+} signals in PAPs, we propose a mathematical model, which incorporates glutamate driven Ca^{2+} responses evoked by simultaneous binding of glutamate to mGluR's and transport of glutamate by GluT while taking the volume ratio of internal Ca^{2+} stores into account. With the help of the model we investigated how the volume ratio between the internal Ca^{2+} store and the intracellular space affects Ca^{2+} signaling evoked on the mGluR- and GluT-dependent pathway in different astrocytic compartments along astrocytic processes from the synapse towards the soma.

Methods

We used a system of ordinary differential equations to describe the changes of the ion concentrations, the membrane voltage and the concentration of IP_3 in a single astrocytic

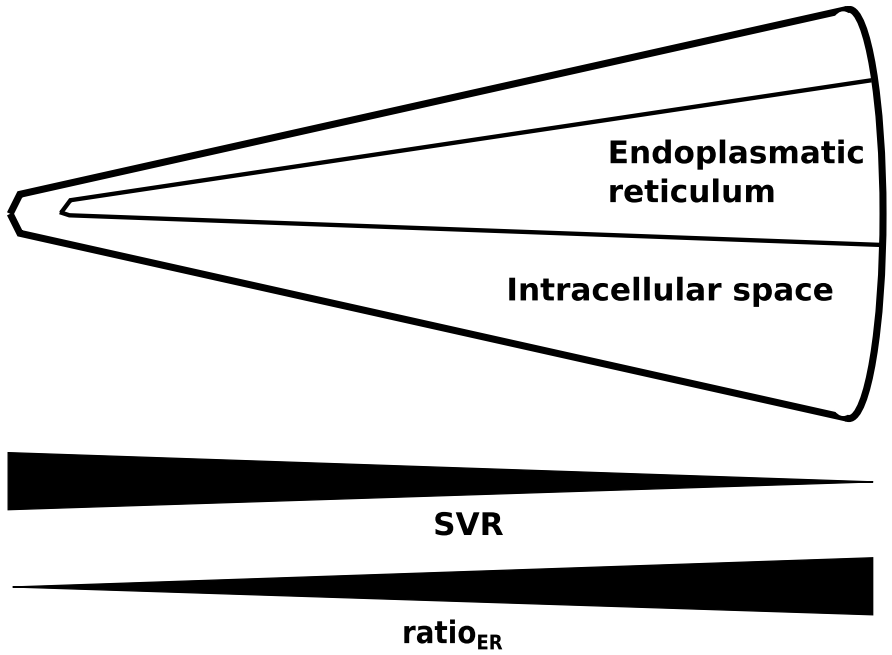

Fig 2. Changes of the astrocytic surface to volume ratio (SVR) and the volume ratio of internal Ca^{2+} stores compared to the intracellular space (ratio$_{ER}$) for astrocytic compartments along the astrocytic process. A small ratio$_{ER}$ corresponds to astrocytic compartments close to the synapse (perisynaptic astrocytic processes (PAPs)) and a high ratio$_{ER}$ corresponds to astrocytic regions at the soma.

doi:10.1371/journal.pcbi.1005377.g002

compartment (see Fig 1) of an astrocytic process. Glutamate dependent Ca^{2+} signals are evoked through two different pathways (see Fig 1). One pathway is driven by the activity of the metabotropic glutamate receptor (mGluR-dependent pathway). The other depends on the activity of the glutamate transporter (GluT-dependent pathway). In the mGluR-dependent pathway glutamate binds to the metabotropic glutamate receptors (mGluR) leading to an enhanced production of the second messenger IP_3 and the subsequent IP_3 dependent Ca^{2+} release from the internal Ca^{2+} store (endoplasmatic reticulum). The exchange of Ca^{2+} between the endoplasmatic reticulum (ER) and the intracellular space is mediated by three currents: the IP_3 receptor current (I_{IP_3R}), which describes the IP_3 dependent Ca^{2+} release from the ER, the Ca^{2+} current of the SERCA pump (I_{Serca}), which transports Ca^{2+} back into the ER, and a Ca^{2+} leak current ($I_{C_{ER}leak}$). The IP_3 receptor channel current is influenced by the concentration of the second messenger IP_3, by the fraction h of active IP_3 receptor channels, and by the Ca^{2+} concentration itself. The GluT-dependent pathway describes the transport of Ca^{2+} through the membrane driven by the activity of the glutamate transporter (GluT). This pathway includes the glutamate transporter, the Na^+/K^+-ATPase (NKA), the Na^+/Ca^{2+} exchanger (NCX), and the Na^+ and K^+ leak currents. The Ca^{2+} transport through the membrane is influenced by the intra- and extracellular Ca^{2+}, Na^+ and K^+ concentrations, and the membrane voltage V.

Geometry of the astrocytic model compartment

We consider small astrocytic compartments, which have a cylindrical shape. Each astrocytic compartment consists of three parts: the internal Ca^{2+} store (endoplasmatic reticulum), the intracellular space, and the extracellular space (see Fig 1). The internal Ca^{2+} store and the

intracellular space are considered as two cylinders with different diameter, which lie within each other. The volume of the intracellular space includes the volume of the internal Ca^{2+} store. The intracellular space is surrounded by the extracellular space. The volume of the extracellular space is set equal to the volume of the intracellular space. Flow of ions to neighboring compartments is not considered. Thus, only the curved surface area of the cylinder is considered.

For the change of the ion concentration within the intracellular space or the internal Ca^{2+} store (see Eq 2), we consider the sum of all ionic currents carrying the respective ion (ΣI_{ion}) multiplied with the area A, the ionic current is flowing through, and divided by the volume Vol of the space the ions are located in. Both A and Vol are scaled by the length l of the compartment. Therefore, the fraction $\frac{A}{Vol}$ does not depend on l and lateral diffusion of ions was neglected.

For each astrocytic compartment the surface area and the volume of both the internal Ca^{2+} store and the intracellular space change along the astrocytic process. The diameter of the intracellular space increases from astrocytic compartments close to the synapse towards astrocytic compartments at the soma (see Fig 2). Thus, the surface area and the volume of the intracellular space increase from the synapse to the soma, but the surface volume ratio (SVR) decreases. The volume ratio between the internal Ca^{2+} store and the intracellular space increases from astrocytic compartments close to the synapse towards astrocytic compartments at the soma. Astrocytic compartments close to the synapse do not contain internal Ca^{2+} stores ($ratio_{ER} = 0$) (see Fig 2).

Within a single astrocytic compartment the diameter of the internal Ca^{2+} store is smaller than the diameter of the intracellular space. The volume of the internal Ca^{2+} store is equal to the volume of the intracellular space reduced by the factor $ratio_{ER}$. Consequently, the surface area of the internal Ca^{2+} store is reduced by the factor $\sqrt{ratio_{ER}}$ compared to the surface area of the intracellular space. Thus, the volume ratio between the internal Ca^{2+} store and the intracellular space determines the change of the surface volume ratio ($SVR = \frac{A}{Vol}$) of the internal Ca^{2+} store along the astrocytic process.

Along the astrocyte process, the surface volume ratio (SVR) and the volume ratio between the internal Ca^{2+} store and the intracellular space depend on each other, and the relationship (see [12] and Fig 3) is quantified by:

$$ratio_{ER} = 0.15 \cdot e^{-(0.002\mu m \cdot SVR)^{2.32}} \tag{1}$$

Dynamics of the ion concentrations, the membrane voltage and the concentration of IP_3

Dynamics of ion concentrations. The change of the ion concentration is given by:

$$\frac{d[ion]}{dt} = \frac{A}{F \cdot Vol} \cdot \sum I_{ion} \tag{2}$$

and depends on the sum of all ionic currents carrying the respective ion (ΣI_{ion}) multiplied with the area (A), the ionic currents are flowing through, and divided by the volume (Vol) of the space the ions are located in and the Faraday constant (F). The change of the intracellular Ca^{2+} concentration is determined by currents crossing either the membrane of the internal Ca^{2+} store or of the outer cell membrane. For that reason the change of the intracellular Ca^{2+}

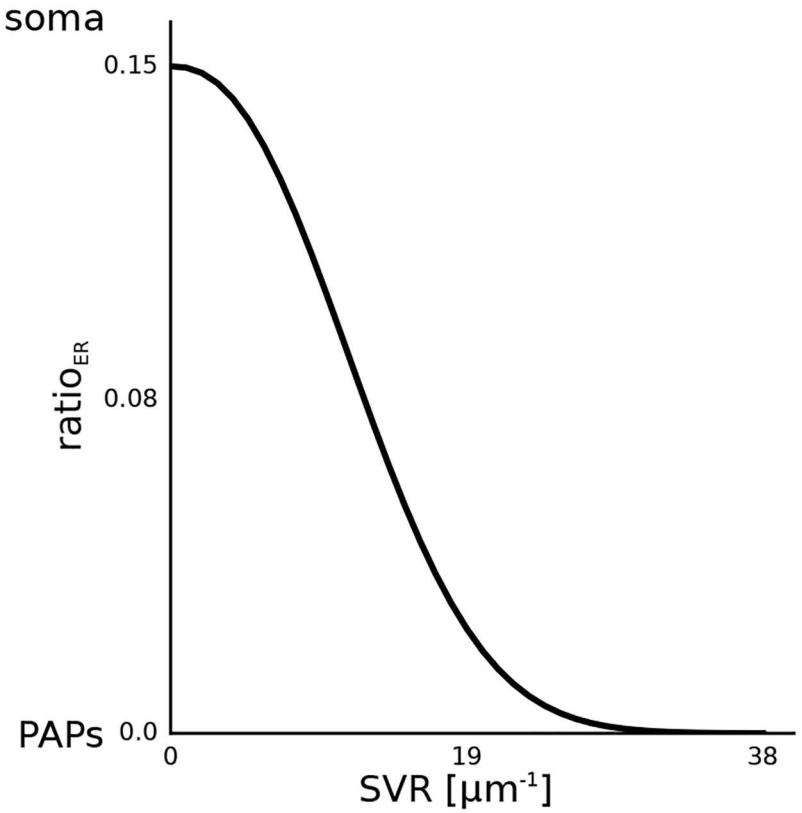

Fig 3. The volume ratio of the endoplasmatic reticulum (ER) as a function of the surface volume ratio (SVR). The data has been adapted from [12].

doi:10.1371/journal.pcbi.1005377.g003

concentration reads as follows:

$$\frac{d[Ca^{2+}]_i}{dt} = \frac{A}{F \cdot Vol} \cdot I_{NCX} + \frac{A \cdot \sqrt{ratio_{ER}}}{F \cdot Vol} \cdot (I_{IP_3R} - I_{Serca} + I_{C_{ER}leak}), \tag{3}$$

where A denotes the area of the outer cell membrane, $A \cdot \sqrt{ratio_{ER}}$ is the area of the internal Ca^{2+} store and the volume of the intracellular space is defined as Vol.

The change of the Ca^{2+} concentration in the ER is determined by currents crossing the membrane of the ER:

$$\frac{d[Ca^{2+}]_{ER}}{dt} = \frac{A \cdot \sqrt{ratio_{ER}}}{F \cdot Vol \cdot ratio_{ER}} \cdot (-I_{IP_3R} + I_{Serca} - I_{C_{ER}leak}),$$

here $A \cdot \sqrt{ratio_{ER}}$ and $Vol \cdot ratio_{ER}$ describe the area and the volume of the internal Ca^{2+} store, respectively.

The change of the intracellular Na^+ and K^+ concentrations are described by the following equations:

$$\frac{d[Na^+]_i}{dt} = \frac{A}{F \cdot Vol} \cdot (3I_{GluT} - 3I_{NKA} - 3I_{NCX} - I_{Na_{leak}})$$
$$\frac{d[K^+]_i}{dt} = \frac{A}{F \cdot Vol} \cdot (-I_{GluT} + 2I_{NKA} - I_{K_{leak}}).$$

Dynamics of the membrane voltage. The change of the membrane voltage V is determined by:

$$\frac{dV}{dt} = -\frac{1}{C_m}(-2I_{IP_3R} + 2I_{Serca} - 2I_{C_{ER}leak} + I_{NCX} - 2I_{GluT} + I_{NKA} + I_{Na_{leak}} + I_{K_{leak}}).$$

The right hand side of the equation consists of the sum of all ionic membrane currents with the consideration of carried charges per ion (see Fig 1). C_m is the membrane capacitance. Note, that the transport of sodium and potassium mediated by the glutamate transporter lead to a net transfer of two positive charges per cycle across the membrane.

Extracellular ion concentrations. The changes of the extracellular Ca^{2+}, Na^+ and K^+ concentrations are determined by:

$$[Ca^{2+}]_o - [Ca^{2+}]_{o_{rest}} = [Ca^{2+}]_i - [Ca^{2+}]_{i_{rest}} + [Ca^{2+}]_{ER_{rest}} - [Ca^{2+}]_{ER} \quad (4)$$

$$[Na^+]_o - [Na^+]_{o\,rest} = [Na^+]_{i\,rest} - [Na^+]_i \quad (5)$$

$$[K^+]_o - [K^+]_{o\,rest} = [K^+]_{i\,rest} - [K^+]_i. \quad (6)$$

We calculated the extracellular concentration as a function of the intracellular concentration under the assumption that the volume of the intracellular and extracellular space of an astrocytic compartment are the same and the overall concentration in the intracellular and the extracellular space of an astrocytic compartment stays constant. Values of model parameters can be found in Table 1.

IP_3 production and degradation. The concentration change of the second messenger IP_3 is determined by the production and degradation of IP_3. The production is mediated by the phosphoinositide-specific phospholipase C β (PLCβ) and the phosphoinositide-specific phospholipase C δ (PLCδ). The degradation is mediated by the IP_3 3-kinase (IP_3-3K) and the

Table 1. Initial values of the ion concentrations, the membrane voltage, IP_3 and the fraction of the activated IP_3 receptor channels. For the calculation of $[Ca^{2+}]_{ER}$, $[IP_3]_i$ and h see Model section **Model parameter values**.

Parameter	Value	Source
$[Ca^{2+}]_i$	0.073 μM	[23]
$[Ca^{2+}]_{ER}$	25 μM	see text
$[Ca^{2+}]_o$	1800 μM	[18]
$[Na^+]_i$	15 mM	[19]
$[Na^+]_o$	145 mM	[19]
$[K^+]_i$	100 mM	[19]
$[K^+]_o$	3 mM	[19]
V	-85 mV	[24]
$[IP_3]_i$	0.15659 μM	see text
h	0.7892	see text

doi:10.1371/journal.pcbi.1005377.t001

inositol polyphosphate 5-phosphatase (IP-5P) [13].

$$\begin{aligned}
\frac{d[IP_3]_i}{dt} &= prod_{PLC\beta} + prod_{PLC\delta} - degr_{IP_3-3K} - degr_{IP-5P} \\
prod_{PLC\beta} &= v_\beta \cdot \frac{g^{0.7}}{g^{0.7} + (K_R + K_p \cdot \frac{[Ca^{2+}]_i}{[Ca^{2+}]_i + K_\pi})^{0.7}} \\
prod_{PLC\delta} &= \frac{v_\delta}{1 + \frac{[IP_3]_i}{\kappa_\delta}} \cdot \frac{[Ca^{2+}]_i^2}{[Ca^{2+}]_i^2 + K_{PLC\delta}^2} \\
degr_{IP_3-3K} &= v_{3K} \cdot \frac{[Ca^{2+}]_i^4}{[Ca^{2+}]_i^4 + K_D^4} \cdot \frac{[IP_3]_i}{[IP_3]_i + K_3} \\
degr_{IP-5P} &= r_{5p} \cdot [IP_3]_i.
\end{aligned}$$

The production of IP_3 by the phosphoinositide-specific phospholipase C (PLC) β is linked to the level of the extracellular glutamate concentration g. The maximal rate of IP_3 production by PLCβ is described by v_β and the glutamate affinity of the receptor is set by K_R. K_p is the Ca^{2+}/PLC-dependent inhibition factor and K_π determines the Ca^{2+} affinity of PLC.

The maximal rate of IP_3 production by PLCδ is described by v_δ. The activity of PLCδ is inhibited according to the inhibition constant k_δ. The Ca^{2+} affinity of PLCδ is set by $K_{PLC\delta}$.

The maximal degradation rate of IP_3 by IP_3-3K is determined by v_{3K}. K_D is the Ca^{2+} affinity of IP_3-3K and K_3 is the IP_3 affinity of IP_3-3K.

The degradation of IP_3 through dephosphorylation by the inositol polyphosphate 5-phosphatase (IP-5P) depends on the maximal rate, r_{5P}, of degradation by IP-5P. Values of model parameters can be found in Table 2.

Table 2. Model parameters for the production and degradation of IP_3. IP_3 production is mediated by PLCβ and PLCδ and IP_3 degradation is mediated by IP_3—3K and IP—5P.

Parameter	Value	Source
IP_3 production by PLCβ		
v_β	0.05 $\frac{\mu M}{s}$	[13]
K_R	1.3 μM	[13]
K_p	10 μM	[13]
K_π	0.6 μM	[13]
IP_3 production by PLCδ		
v_δ	0.02 $\frac{\mu M}{s}$	[13]
k_δ	1.5 μM	[13]
$K_{PLC\delta}$	0.1 μM	[13]
IP_3 degradation by IP_3—3K		
v_{3K}	2 $\frac{\mu M}{s}$	[13]
K_D	0.7 μM	[13]
K_3	1 μM	[13]
IP_3 degradation by IP—5P		
r_{5P}	0.04 $\frac{1}{s}$	[13]

doi:10.1371/journal.pcbi.1005377.t002

Table 3. Model parameters for the Ca^{2+} currents through the membrane of the endoplasmatic reticulum: The IP_3 receptor channel, the SERCA pump and the Ca^{2+} leak current.

Parameter	Value	Source
IP_3 receptor channel		
r_C	$6\,\frac{1}{s}$	[13]
d_1	0.13 μM	[13]
d_5	0.08234 μM	[13]
SERCA pump		
v_{ER}	$4\,\frac{\mu M}{s}$	[25, 26]
K_{ER}	0.1 μM	[13]
Ca^{2+} leak		
r_L	$0.11\,\frac{1}{s}$	[13]

doi:10.1371/journal.pcbi.1005377.t003

Currents

Intracellular dynamics. *Ca^{2+} current through IP_3 receptor channels.* The Ca^{2+} current through the IP_3 receptor channel was taken from [14]:

$$I_{IP_3R} = \frac{F \cdot Vol}{A} \cdot r_C \cdot \left(\frac{[IP_3]_i}{[IP_3]_i + d_1}\right)^3 \cdot \left(\frac{[Ca^{2+}]_i}{[Ca^{2+}]_i + d_5}\right)^3 \cdot h^3 \cdot ([Ca^{2+}]_{ER} - [Ca^{2+}]_i). \quad (7)$$

r_C determines the maximal rate of transported Ca^{2+} ions. The dissociation of IP_3 and Ca^{2+} by the channels' subunits is determined by d_1 and d_5.

The probability of the channel to be in the open state is characterized by the term $\left(\frac{[IP_3]_i}{[IP_3]_i+d_1}\right)^3 \cdot \left(\frac{[Ca^{2+}]_i}{[Ca^{2+}]_i+d_5}\right)^3 \cdot h^3$ and depends on the intracellular IP_3 concentration, the intracellular Ca^{2+} concentration and the fraction h of activated IP_3 receptor channels. The channel can either be in the activated or the inactivated state. As proposed in [14] the channel is in the activated state when one Ca^{2+} ion and one IP_3 molecule bind to two out of the three subunits of the channel. The channel is in the inactivated state when a second Ca^{2+} ion binds to the third subunit. The current strength is proportional to the Ca^{2+} gradient between the ER and the intracellular space, ($[Ca^{2+}]_{ER}$—$[Ca^{2+}]_i$). In order to relate the current strength to the volume of the intracellular space, the current is multiplied with the volume *Vol*. The current is normalized by the area *A*. Values of model parameters can be found in Table 3.

Activation of IP_3 receptor channels. The fraction h of activated IP_3 receptor channels was taken from [14],

$$\frac{dh}{dt} = a_2 \cdot \left(d_2 \cdot \frac{[IP_3]_i + d_1}{[IP_3]_i + d_3} \cdot (1 - h) - h \cdot [Ca^{2+}]_i\right) \quad (8)$$

a_2 determines the IP_3R binding rate for Ca^{2+} inhibition. The inactivation dissociation constants of Ca^{2+} and IP_3 are d_2 and d_3, respectively. Values of model parameters can be found in Table 4.

Table 4. Model parameters for the dynamics of the fraction h of activated IP_3 receptor channels.

Parameter	Value	Source
a_2	$0.2\,\frac{1}{s}$	[13]
d_2	1.049 μM	[13]
d_3	0.9434 μM	[13]

doi:10.1371/journal.pcbi.1005377.t004

SERCA pump. The transport of Ca^{2+} ions into the endoplasmatic reticulum mediated by the SERCA pump was taken from [14],

$$I_{Serca} = \frac{F \cdot Vol}{A} \cdot \upsilon_{ER} \cdot \frac{[Ca^{2+}]_i^2}{[Ca^{2+}]_i^2 + K_{ER}^2}. \quad (9)$$

The maximal rate of Ca^{2+} uptake by the SERCA pump is determined by v_{ER}. K_{ER} determines the Ca^{2+} affinity of the SERCA pump. In order to relate the current strength to the volume of the intracellular space, the current is multiplied with the volume *Vol*. The current is normalized by the area *A*.

The SERCA current depends on the intracellular Ca^{2+} concentration $[Ca^{2+}]_i$ and is modeled by a Hill rate expression with an exponent 2. Values of model parameters can be found in Table 3.

Ca^{2+} leak from the ER. The Ca^{2+} leak from the endoplasmatic reticulum was taken from [14]:

$$I_{C_{ER}leak} = \frac{F \cdot Vol}{A} \cdot r_L \cdot ([Ca^{2+}]_{ER} - [Ca^{2+}]_i), \quad (10)$$

where r_L is the leak rate.

The leak of Ca^{2+} ions from the endoplasmatic reticulum into the cytosol depends on the difference of the Ca^{2+} concentration in the ER, $[Ca^{2+}]_{ER}$, and in the intracellular space $[Ca^{2+}]_i$. In order to relate the current strength to the volume of the intracellular space, the current is multiplied with the volume *Vol*. The current is normalized by the area *A*. Values of model parameters can be found in Table 3.

Transmembrane transporters. *Glutamate transporter*. The transport of glutamate mediated by the glutamate transporter (GluT) is determined by:

$$I_{GluT} = I_{GluT_{max}} \cdot \frac{[K^+]_i}{[K^+]_i + K_{GluT_{mK}}} \cdot \frac{[Na^+]_o^{\,3}}{[Na^+]_o^{\,3} + K_{GluT_{mN}}^{\,3}} \cdot \frac{g}{g + K_{GluT_{mg}}}, \quad (11)$$

where $I_{GluTmax}$ is the maximal transport current of the glutamate transporter. The half saturation constants of Na^+, K^+ and glutamate are given by K_{GluTmN}, K_{GluTmK} and K_{GluTmg}, respectively. The half saturation constant of K^+ is not known from experiments. Since the half saturation constant of Na^+ is close to its intracellular resting concentration, we set the half saturation constant of K^+ close to its extracellular resting concentration.

The transport of glutamate is coupled to the co-transport of three Na^+, one Glu^- and one H^+, and the counter-transport of one K^+ [15, 16]. It results in a net flux of two positive charges per cycle, which is included in the calculation of the membrane potential. The concentrations of H^+ and Glu^- in the different compartments, however, are excluded from the model, because they do not influence any of the other model variables under consideration. Values for the model parameters are listed in Table 5. Additionally, there is a non-stochiometric anion (Cl^-) current coupled to the glutamate transporter [17]. Inclusion of this current into the equation for the membrane voltage, however, led to minor changes in the simulation results, as long as its maximum conductance was chosen with a physiologically reasonable range ($10^{-7}\ \frac{nS}{\mu m^2}$). It was, therefore, not considered further.

Na^+/K^+-ATPase. The transport of Na^+ and K^+ against its concentration gradient is performed by the Na^+/K^+-ATPase (NKA). We applied the mathematical expression of [18] in a

Table 5. Model parameters for the currents through the plasma membrane: The glutamate transporter, the Na^+/K^+ ATPase, the Na^+/Ca^{2+} exchanger and the leak currents for Na^+ and K^+. The determination of the model parameters $I_{GluTmax}$ and I_{NKAmax} can be found in the Results section **Na^+ transport by the glutamate transporter**. The definition of the model parameter K_{GluTmK} can be found in the Model section **Glutamate Transporter**. For the calculation of g_{Naleak} and g_{Kleak} see Model section **Model parameter values**.

Parameter	Value	Source
Glutamate Transporter		
$I_{GluTmax}$	0.68 $\frac{pA}{\mu m^2}$	see text
K_{GluTmN}	15 mM	[27]
K_{GluTmK}	5 mM	see text
K_{GluTmg}	34 μM	[27]
Na^+/K^+ ATPase		
I_{NKAmax}	1.52 $\frac{pA}{\mu m^2}$	see text
K_{NKAmN}	10 mM	[18]
K_{NKAmK}	1.5 mM	[18]
Na^+/Ca^{2+} exchanger		
I_{NCXmax}	0.1 $\frac{pA}{\mu m^2}$	see text
K_{NCXmN}	87500 μM	[18]
K_{NCXmC}	1380 μM	[18]
k_{sat}	0.1	[18]
η	0.35	[18]
Leak Currents		
g_{Naleak}	0.0065 $\frac{nS}{\mu m^2}$	see text
g_{Kleak}	0.0791 $\frac{nS}{\mu m^2}$	see text

doi:10.1371/journal.pcbi.1005377.t005

simplified form:

$$I_{NKA} = I_{NKA_{max}} \cdot \frac{[Na^+]_i^{1.5}}{[Na^+]_i^{1.5} + K_{NKA_{mN}}^{1.5}} \cdot \frac{[K^+]_o}{[K^+]_o + K_{NKA_{mK}}}. \quad (12)$$

Here, I_{NKAmax} defines the maximal pumping activity of the NKA. K_{NKAmN} and K_{NKAmK} determine the half saturation constants of Na^+ and K^+, respectively.

The Na^+/K^+-ATPase (NKA) transports three Na^+ ions out of the cell and two K^+ ions into the cell. Its pumping activity depends on the intracellular Na^+ concentration $[Na^+]_i$ and the extracellular K^+ concentration $[K^+]_o$ [19]. Values of model parameters can be found in Table 5.

Na^+/Ca^{2+} exchanger. The Na^+/Ca^{2+} exchanger (NCX) mediates the exchange of three Na^+ ions with one Ca^{2+} ion. We applied the mathematical description of the NCX of [18]:

$$I_{NCX} = I_{NCX_{max}} \cdot \frac{[Na^+]_o^3}{K_{NCXmN}^3 + [Na^+]_o^3} \cdot \frac{[Ca^{2+}]_o}{K_{NCXmC} + [Ca^{2+}]_o} \cdot \frac{\frac{[Na^+]_i^3}{[Na^+]_o^3} \cdot exp\left(\eta \cdot \frac{V \cdot F}{R \cdot T}\right) - \frac{[Ca^{2+}]_i}{[Ca^{2+}]_o} \cdot exp\left((\eta - 1) \cdot \frac{V \cdot F}{R \cdot T}\right)}{1 + k_{sat} \cdot exp\left((\eta - 1) \cdot \frac{V \cdot F}{R \cdot T}\right)} \quad (13)$$

I_{NCXmax} is the maximal pump current of the exchanger. The half saturation constants for Na^+

and Ca^{2+} are given by K_{NCXmN} and K_{NCXmC}. The position of the energy barrier η controls the voltage dependence. k_{sat} is a saturation factor ensuring saturation at large negative potentials.

The exchanger works either in the forward or in the reverse mode. In the forward mode Ca^{2+} is transported out of the astrocyte and Na^+ is transported into the astrocyte. The reverse mode works the other way round. A switch into the reverse mode is induced by an increased intracellular Na^+ concentration [20]. The current strength of the NCX depends on the intra- and extracellular Na^+ and Ca^{2+} concentrations $[Na^+]_i$, $[Na^+]_o$, $[Ca^{2+}]_i$ and $[Ca^{2+}]_o$. Values of model parameters can be found in Table 5.

Leak currents. The leak currents of Na^+ and K^+ are given by:

$$I_{Na_{leak}} = g_{Na_{leak}} \cdot (V - E_{Na}) \tag{14}$$

$$I_{K_{leak}} = g_{K_{leak}} \cdot (V - E_K), \tag{15}$$

where $g_{Na_{leak}}$ and $g_{K_{leak}}$ are the corresponding conductances of the Na^+ and K^+ currents. The Nernst potentials of Na^+ and K^+ are E_{Na} and E_K. Values of model parameters can be found in Table 5.

Neuronal stimulation of the astrocyte compartment

The release of glutamate from an activated nearby synapse is calculated using the Tsodykis and Makram model [21, 22] in its adapted form published by Wallach and colleagues [7].

$$\begin{aligned} r(t) &= x(t) \cdot y(t) \\ \frac{dx}{dt} &= \frac{(1 - x(t))}{\tau_{rec}} - x(t) \cdot y(t) \cdot s(t) \\ \frac{dy}{dt} &= -\frac{y(t)}{\tau_{facil}} + U_0(1 - y(t)) \cdot s(t) \\ \frac{dg}{dt} &= -\frac{g}{\tau_{clear}} + \rho_C G_T \cdot r(t), \end{aligned}$$

where x and y represent the fraction of resources in the recovered and active states, respectively. During each spike a fraction of active synaptic resources is released into the synaptic cleft, and the time constant τ_{rec} determines the recovery of these resources. The fraction of active synaptic resources y increases with each spike and the step increase of y is determined by U_0. In the absence of a spike y decays back to a baseline level with time constant τ_{facil}. The product $r(t)$ corresponds to the ratio of glutamate (g) which is released during a spike of the sequence s. The change of the glutamate concentration in the synaptic cleft is determined by the total glutamate content of readily releasable vesicles (G_T) and the volume ratio between the synaptic vesicles and the synaptic cleft (ρ_C). Glutamate is removed from the synaptic cleft with the time constant τ_{clear}. Values of model parameters can be found in Table 6.

Table 6. Parameters for the Tsodyks and Markram model.

Parameter	Value	Source
τ_{facil}	$2\ s^{-1}$	[7]
τ_{rec}	$1\ s^{-1}$	[7]
τ_{clear}	$60\ s^{-1}$	[7]
U_0	0.25	[7]
ρ_C	$6.5 \cdot 10^{-4}$	[7]

doi:10.1371/journal.pcbi.1005377.t006

Model parameter values

The initial values of $[IP_3]_i$, the fraction h of active IP_3 receptor channels, and $[Ca^{2+}]_{ER}$ and the model parameters g_{Naleak} and g_{Kleak} were determined as follows. Since the model parameters for the production and degradation of IP_3 and the intracellular resting concentration of Ca^{2+} were known from literature, the zero of $d[IP_3]_i/dt$ revealed the initial concentration of IP_3. In the same way the initial ratio of activated IP_3 receptor channels, h, and the initial concentration of the Ca^{2+} concentration in the endoplasmatic reticulum was calculated. In this way a stable resting state was ensured. The model parameter g_{Naleak} was calculated by setting $d[Na^+]_i/dt$ equal to zero and solving the equation for g_{Naleak}. The model parameter g_{Kleak} was calculated the same way by setting $d[K^+]_i/dt$ equal to zero.

Computational methods

All simulations were performed with Python 2.7 using the packages Brian [28], NumPy and Matplotlib. The Brian Simulator used the Euler integration as numerical integration method for the non-linear differential equations with time step dt = 1ms.

Results

Influence of $ratio_{ER}$ on the mGluR-driven Ca^{2+} oscillations

First, we analyzed the generation of mGluR-dependent Ca^{2+} signals along the astrocytic process. For this reason we varied the volume fraction of the internal Ca^{2+} store ($ratio_{ER}$), which changes along the astrocytic process (Fig 3), and studied the amplitude and the frequency of the Ca^{2+} signals (Fig 4). All currents related to the GluT-dependent pathway (I_{GluT}, I_{NKA}, I_{NCX}) were set to zero.

Astrocytic compartments with a high volume fraction of the internal Ca^{2+} store ($ratio_{ER}>0.06$) showed Ca^{2+} oscillations (Fig 4b). These compartments corresponded to astrocytic regions close to the soma. A reduction of $ratio_{ER}$ decreased the amplitude of the Ca^{2+} oscillations. This was caused by the weaker Ca^{2+} influx into the cytoplasm through the smaller surface area of the internal Ca^{2+} store. Astrocytic compartments closer to the synapse ($0<ratio_{ER}<0.06$) did not show Ca^{2+} oscillations, but an increase of the intracellular Ca^{2+} concentration. However, when the astrocytic compartment was devoid of the internal Ca^{2+} store ($ratio_{ER} = 0$), we observed an unchanged intracellular Ca^{2+} concentration. Different stimulation frequencies led to qualitatively similar behavior (data not shown). In particular, the critical value of $ratio_{ER} = 0.06$ for the onset of oscillations remained the same.

Na^+ transport by the glutamate transporter of the GluT-dependent pathway

The Ca^{2+} entry through the plasma membrane mediated by the Na^+/Ca^{2+} exchanger is driven by a Na^+ accumulation in the intracellular space. The glutamate transporter (GluT), the Na^+/Ca^{2+} exchanger (NCX) and the Na^+-K^+-ATPase (NKA) determine the intracellular Na^+ concentration. For this reason we analyzed the increase of the intracellular Na^+ concentration as a function of the maximal pump currents of the glutamate transporter ($I_{GluTmax}$), the Na^+-K^+-ATPase (I_{NKAmax}), and the Na^+/Ca^{2+} exchanger (I_{NCXmax}).

The maximal pump current of the GluT ($I_{GluTmax}$) and the NKA (I_{NKAmax}) had a strong effect on the accumulation of Na^+ in the astrocyte, while changes of the maximal pump current of the NCX (I_{NCXmax}) showed no effect (see Fig 5). The accumulation of Na^+ in the intracellular space was highest for a high maximal pump current of GluT and a low maximal pump current of NKA (see Fig 5a). While the GluT transported Na^+ into the astrocyte, the NKA

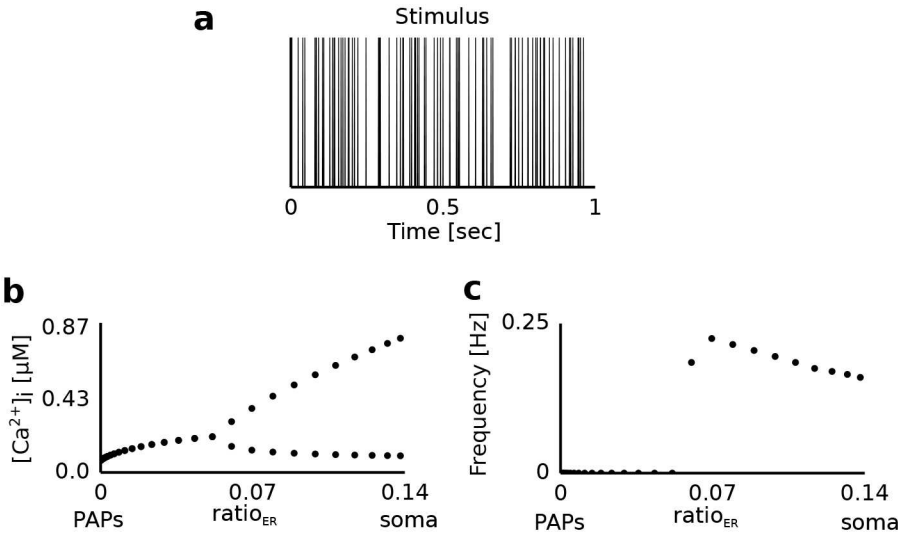

Fig 4. Dynamics of the Ca^{2+} concentration in the intracellular compartment during synaptic activation. a Sample stimulus (spikes). The astrocytic compartment was stimulated for 200 seconds with a Poisson spike train of 100 Hz. The corresponding glutamate concentration in the extracellular compartment as a function of time was calculated using the Tsodyks-Markram model. **b** $[Ca^{2+}]_i$ for different values of the volume ratio ($ratio_{ER}$) between the internal Ca^{2+} store and the intracellular compartments. The upper and lower symbols for $ratio_{ER}>0.06$ denote the average height of peaks and troughs of the emerging Ca^{2+} oscillations (in [μM]). For $ratio_{ER}\leq 0.06$ no Ca^{2+} oscillations were present and symbols denote the average concentration of Ca^{2+} over the stimulation period. **c** Frequency of Ca^{2+} oscillations as a function of $ratio_{ER}$.

doi:10.1371/journal.pcbi.1005377.g004

counteracted this effect by pumping Na^+ out of the astrocyte and led to a saturation of $[Na^+]_i$ at lower concentration levels. The time until saturation was lowest for a low maximal pump current of the GluT and a high maximal pump current of the NKA (see Fig 5b). A low maximal pump current of the GluT resulted in a small Na^+ accumulation in the intracellular space, which saturated faster for a high Na^+ transport out of the astrocyte mediated by the NKA.

In experiments the increase of the intracellular Na^+ concentration in response to external stimulation with glutamate ranges from 10 mM to 20 mM saturating with increasing glutamate concentrations [29] and is performed in under 60 seconds [30]. For the following simulations we chose a parameter combination of the maximal pump currents of the GluT and the NKA which revealed the desired results for the increase of the intracellular Na^+ concentration and the time to saturation ($I_{GluTmax} = 0.68\ \frac{pA}{\mu m^2}$ and $I_{NKAmax} = 1.52\ \frac{pA}{\mu m^2}$.).

Ca^{2+} transport through the plasma membrane

As a next step, we analyzed how the Ca^{2+} transport through the membrane mediated on the GluT-dependent pathway affects mGluR-dependent Ca^{2+} signals along the astrocytic process. Different regions of the astrocytic process were simulated by changing the volume fraction of the internal Ca^{2+} store ($ratio_{ER}$). We analyzed the influence of the GluT-dependent pathway on the Ca^{2+} signal by changing the maximal pump currents of the Na^+/Ca^{2+} exchanger (I_{NCXmax}) and the glutamate transporter ($I_{GluTmax}$).

First, we analyzed the impact of Ca^{2+} transport through the membrane mediated by the Na^+/Ca^{2+} exchanger on the intracellular Ca^{2+} signal along the astrocytic process (see Fig 6). During a block of the Ca^{2+} transport through the membrane ($I_{NCXmax} = 0\ \frac{pA}{\mu m^2}$) Ca^{2+} oscillations were only observed for a high volume fraction of the internal Ca^{2+} store ($ratio_{ER}>0.06$) (see Fig 6a and 6g). An increase of the maximal pump current of the Na^+/Ca^{2+} exchanger

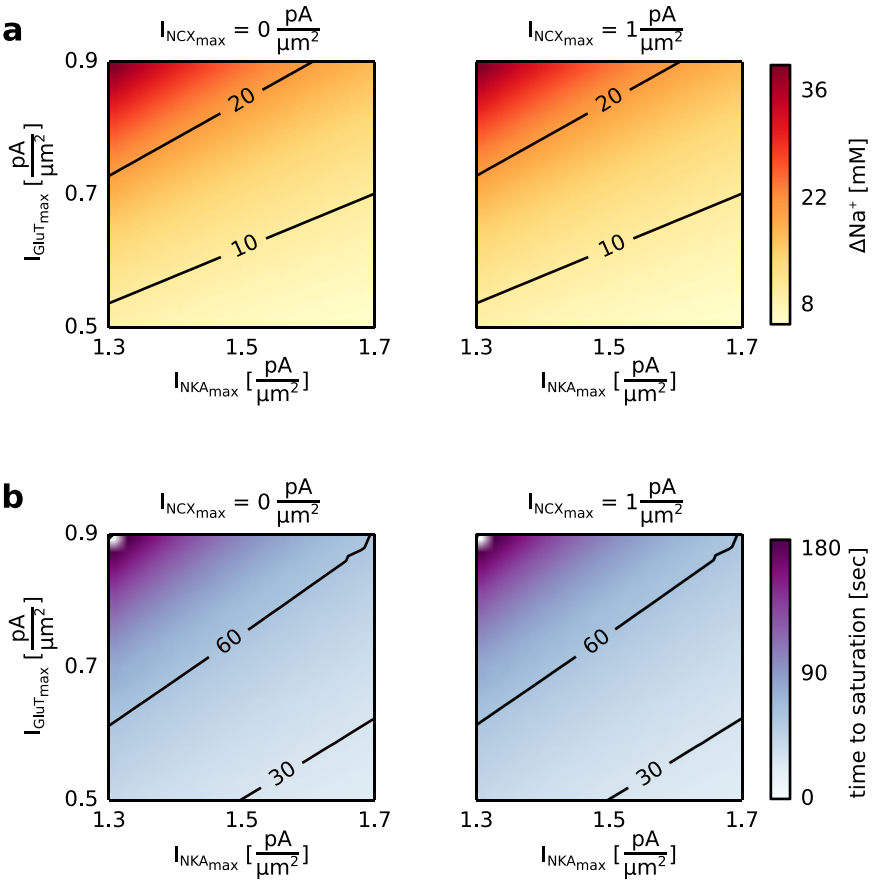

Fig 5. Increase of the Na^+ concentration in the intracellular compartment, $[Na^+]_i$, during a constant extracellular glutamate concentration for different values of the maximal pump currents of the Na^+/Ca^{2+} exchanger (I_{NCXmax}), the glutamate transporter ($I_{GluTmax}$), the Na^+/K^+-ATPase (I_{NKAmax}). The astrocytic compartment was stimulated for 200 seconds with a constant extracellular glutamate concentration of 100 μM. The surface volume ratio (SVR) was set equal to 1 μm^{-1}, which corresponds to astrocytic compartments close to the soma. **a** $[Na^+]_i$ after 200 seconds with respect to its resting concentration ($[Na^+]_{rest}$ = 15 mM, $\Delta Na^+ = [Na^+]_{End} - [Na^+]_{rest}$) for a maximal pump current of the Na^+/Ca^{2+} exchanger (I_{NCXmax}) equal to 0 $\frac{pA}{\mu m^2}$ (left) or equal to 1 $\frac{pA}{\mu m^2}$ (right) and different values of the maximal pump current of the glutamate transporter ($I_{GluTmax}$) and the Na^+/K^+-ATPase (I_{NKAmax}). **b** Time to reach saturation for a maximal pump current of the Na^+/Ca^{2+} exchanger (I_{NCXmax}) equal to 0 $\frac{pA}{\mu m^2}$ (left) or equal to 1 $\frac{pA}{\mu m^2}$ (right) and different values of the maximal pump current of the glutamate transporter ($I_{GluTmax}$) and the Na^+/K^+-ATPase (I_{NKAmax}). The time to saturation was defined as the time required for the intracellular Na^+ concentration to remain on a constant concentration.

doi:10.1371/journal.pcbi.1005377.g005

($I_{NCXmax} > 0 \frac{pA}{\mu m^2}$) shifted the critical value of $ratio_{ER}$ for the onset of Ca^{2+} oscillations to higher values (see Fig 6a), culminating in a total suppression of the Ca^{2+} oscillations (see Fig 6e). In astrocytic compartments, which were devoid of the internal Ca^{2+} store ($ratio_{ER} = 0$), Ca^{2+} was transported into the astrocyte and the intracellular Ca^{2+} concentration increased (see Fig 6b and 6c).

Second, we analyzed the influence of the maximal pump current of the glutamate transporter ($I_{GluTmax}$) on the Ca^{2+} signal (see Fig 7). The impact of $I_{GluTmax}$ on the Ca^{2+} signal mainly depended on the maximal pump current of the Na^+/Ca^{2+} exchanger (I_{NCXmax}) and the volume fraction of the internal Ca^{2+} store ($ratio_{ER}$). In astrocytic compartments close to the soma ($ratio_{ER} \geq 0.1$) an increase of $I_{GluTmax}$ increased the Ca^{2+} oscillation frequency until it

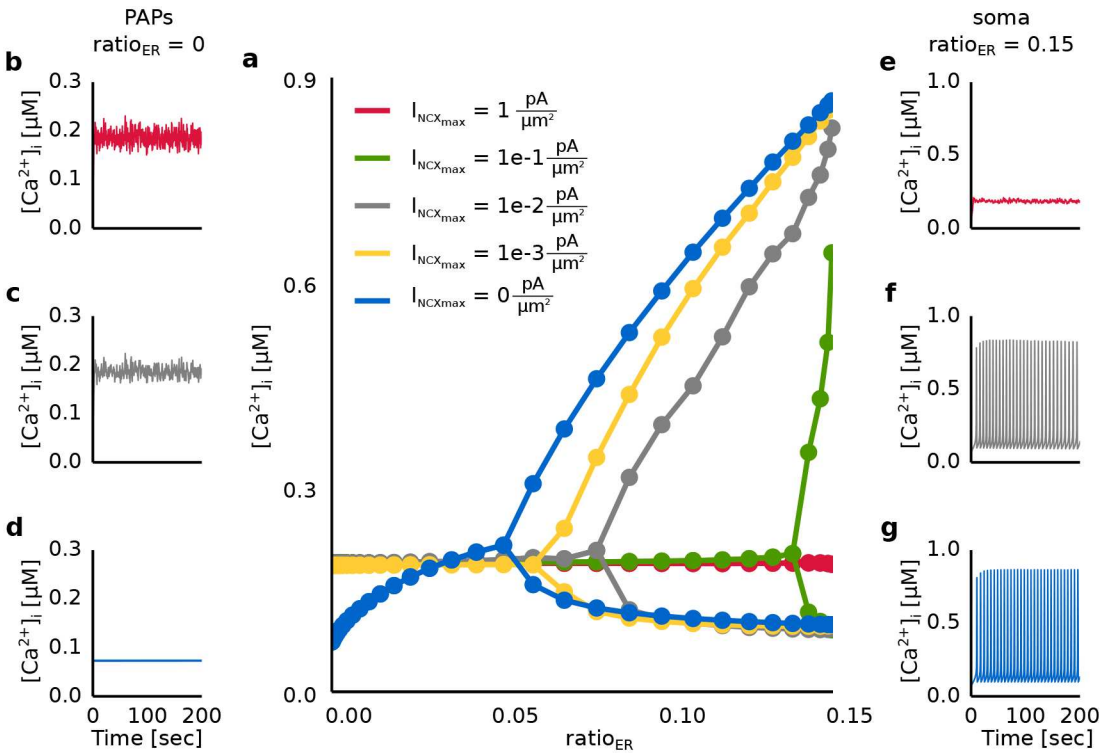

Fig 6. Dynamics of the Ca^{2+} concentration in the intracellular compartment during synaptic activation for different values of the maximal pump current of the Na^+/Ca^{2+} exchanger (I_{NCXmax}). The astrocytic compartment was stimulated for 200 seconds with a Poisson spike train of 100 Hz. The corresponding glutamate concentration in the extracellular compartment as a function of time was calculated using the Tsodyks and Markram model. **a** $[Ca^{2+}]_i$ as a function of the volume ratio ($ratio_{ER}$) of internal Ca^{2+} stores and the maximal pump current of the Na^+/Ca^{2+} exchanger (I_{NCXmax}). The upper and lower symbols denote the average height of peaks and troughs of the emerging Ca^{2+} oscillations (in [μM]). In case no oscillations were present symbols denote the average concentration of Ca^{2+} over the stimulation period. **b-d** Time course of the Ca^{2+} concentration for $ratio_{ER} = 0$ and I_{NCXmax} equal to 0 $\frac{pA}{\mu m^2}$ (blue), 0.01 $\frac{pA}{\mu m^2}$(gray) and 1 $\frac{pA}{\mu m^2}$(red). **e-g** Time course of the Ca^{2+} concentration for $ratio_{ER} = 0.15$ and I_{NCXmax} equal to 0 $\frac{pA}{\mu m^2}$ (blue), 0.01 $\frac{pA}{\mu m^2}$(gray) and 1 $\frac{pA}{\mu m^2}$(red).

doi:10.1371/journal.pcbi.1005377.g006

reached a maximal value and decreased again (see Fig 7a and 7b). An increase of I_{NCXmax} shifted the maximal value of the oscillation frequency to lower values of $I_{GluTmax}$ (see Fig 7a). The increase of $I_{GluTmax}$ caused a higher increase of the intracellular Na^+ concentration. The higher Na^+ accumulation activated the Na^+/Ca^{2+} exchanger in the reverse mode and prevented an outflux of Ca^{2+} into the extracellular space. The elevated Ca^{2+} transport into the cell preserved the Ca^{2+} oscillations for high values of I_{NCXmax} and resulted in an increase of the oscillation frequency. The amplitude of the Ca^{2+} oscillations was mainly affected by the volume fraction of internal Ca^{2+} stores and increased with an increase of $ratio_{ER}$ (see Fig 7c). The increase of the volume of both the internal Ca^{2+} store and the intracellular space with $ratio_{ER}$ caused an enhanced Ca^{2+} release from the internal Ca^{2+} store.

The interplay of the mGluR- and GluT-dependent pathways showed the experimentally observed Ca^{2+} fluctuations in astrocytic compartments with a low volume fraction of an internal Ca^{2+} store ($ratio_{ER}$) for a high pumping activity of the NCX ($I_{NCXmax} > 0$ $\frac{pA}{\mu m^2}$). However, a high maximal pump current of the NCX ($I_{NCXmax} > 0.01$ $\frac{pA}{\mu m^2}$) evoked a suppression of the Ca^{2+} oscillations in regions with a high $ratio_{ER}$. Thus, in comparison with experimental data the simulation data suggested a low maximal pump current of the NCX for regions with a high

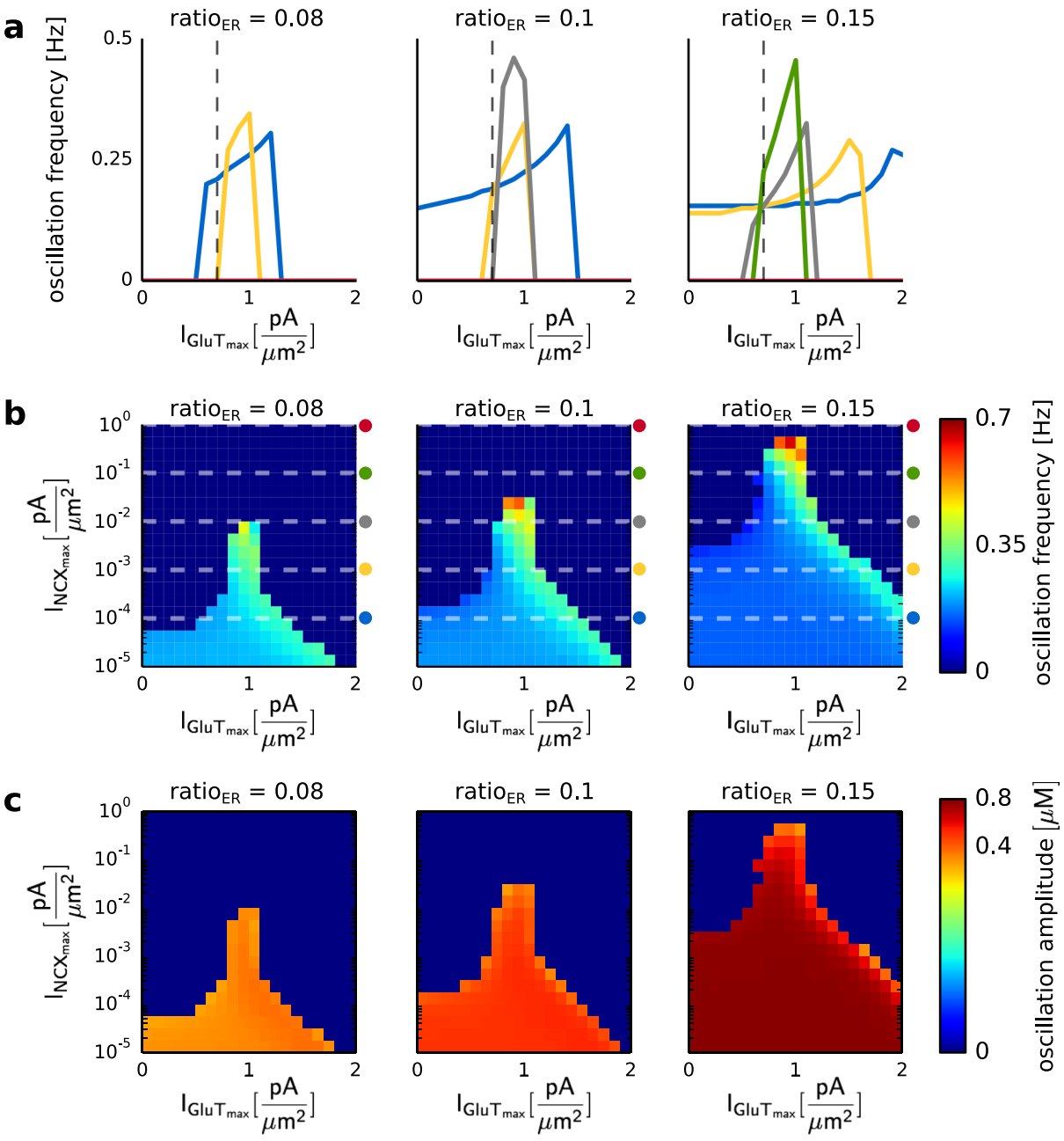

Fig 7. Ca^{2+} oscillation frequency and amplitude for different values of the volume ratio between the internal Ca^{2+} store and the intracellular space ($ratio_{ER}$), as well as the maximal pump currents of the Na^+/Ca^{2+} exchanger ($I_{NCX_{max}}$) and the glutamate transporter ($I_{GluT_{max}}$). The astrocytic compartment was stimulated for 200 seconds with a Poisson spike train of 100 Hz. **a** Ca^{2+} oscillation frequency for three different values of $ratio_{ER}$ (0.08, 0.1 and 0.15), as a function of $I_{GluT_{max}}$ and $I_{NCX_{max}}$. The colored lines correspond to $I_{NCX_{max}}$ equal to $0.0001\frac{pA}{\mu m^2}$ (blue), $0.001\frac{pA}{\mu m^2}$ (yellow), $0.01\frac{pA}{\mu m^2}$ (gray), $0.1\frac{pA}{\mu m^2}$ (green) and $1\frac{pA}{\mu m^2}$ (red). The dashed line corresponds to $I_{GluT_{max}}$ equal to $0.68\frac{pA}{\mu m^2}$. **b** Ca^{2+} oscillation frequencies for three different values of $ratio_{ER}$ (0.08 0.1 and 0.15), as a function of $I_{GluT_{max}}$ and $I_{NCX_{max}}$. The colored symbols denote the values of $I_{NCX_{max}}$ shown in **a**. **c** Ca^{2+} oscillation amplitudes for four different values of $ratio_{ER}$ (0.05, 0.06, 0.1 and 0.15), and as a function of $I_{GluT_{max}}$ and $I_{NCX_{max}}$.

doi:10.1371/journal.pcbi.1005377.g007

$ratio_{ER}$ and a high maximal pump current of the NCX in regions with a small $ratio_{ER}$. Moreover, an increase of $I_{GluTmax}$ allowed Ca^{2+} oscillations for high values of I_{NCXmax} ($I_{NCXmax} \geq 1 \frac{pA}{\mu m^2}$). Thus, the distribution of GluTs and NCXs determines Ca^{2+} signal along the astrocytic process. The reason for the suppression of the Ca^{2+} oscillations for high $ratio_{ER}$ was investigated in a later results section.

Impact of the GluT activity on the Ca^{2+} response under synaptic stimulation

Experiments have shown that a block of the glutamate transporter (GluT) leads to a clear attenuation of the Ca^{2+} signal [8]. For that reason we examined the impact of the GluT-driven Ca^{2+} signal on the overall Ca^{2+} response to synaptic stimulation. Fig 8 shows the dynamics of the Ca^{2+} signal as a function of the volume ratio between the internal Ca^{2+} store and the intracellular space ($ratio_{ER}$) with ('control condition') and without ('block') a contribution of the GluT.

We observed a high impact of the GluT-driven Ca^{2+} signal for a high pumping activity of the Na^+/Ca^{2+} exchanger ($I_{NCXmax} > 0.1 \frac{pA}{\mu m^2}$) and a small volume ratio between the internal Ca^{2+} store and the intracellular space ($ratio_{ER}<0.1$) (see Fig 8b and 8e). With a decrease of I_{NCXmax} and an increase of $ratio_{ER}$ the impact of the GluT-driven Ca^{2+} signal decreased (see Fig 8b, 8c and 8d). In astrocytic compartments with a low volume fraction of the internal Ca^{2+} store the Ca^{2+} signal mainly arose by the Ca^{2+} transported through the membrane (see Fig 4). A block of the glutamate transporter prevented a Na^+ accumulation in the intracellular space (see S1 Fig). The Na^+/Ca^{2+} exchanger remained in the forward mode and transported Ca^{2+} out of the astrocyte. Thus, during a block of the glutamate transporter no Ca^{2+} was transported into the astrocyte via the Na^+/Ca^{2+} exchanger and a clear attenuation of the Ca^{2+} signal was observed in regions with a small $ratio_{ER}$. With an increase of the volume fraction of the internal Ca^{2+} store more Ca^{2+} was released from the internal Ca^{2+} store and led to a lower impact of the glutamate transporter on the overall Ca^{2+} signal. The extracellular glutamate concentration and the Ca^{2+} entry through the membrane affected the IP_3 production as well as the IP_3- and Ca^{2+}-dependent Ca^{2+} release from internal Ca^{2+} stores. An increase of $ratio_{ER}$ was accompanied with an increase of the IP_3- and Ca^{2+}-dependent Ca^{2+} release from internal Ca^{2+} stores and thus with an increase of the impact of the mGluR-dependent mechanism. For that reason, Ca^{2+} signals mainly evoked by the GluT-dependent mechanism were observed in regions with a small $ratio_{ER}$.

Interaction of the mGluR-dependent and GluT-dependent pathway

In order to study the mechanisms underlying the interaction of the mGluR- and GluT-dependent pathways we analyzed the Ca^{2+} concentration in the three spaces as well as the concentration of IP_3 in the intracellular space and the fraction h of open IP_3 channels for different values of the maximal pump current of the Na^+/Ca^{2+} exchanger (I_{NCXmax}) and the volume ratio of internal Ca^{2+} stores ($ratio_{ER}$). Fig 9 summarizes the results. Oscillations of the Ca^{2+} concentration in the intracellular compartment (see Fig 9b) were reflected in all of the other dynamical variables (see Fig 9c–9f). When the GluT-dependent pathway was studied in isolation and Ca^{2+} release from internal Ca^{2+} stores was neglected (see Fig 9a) a finite current through the Na^+/Ca^{2+} exchanger led to an increase of $[Ca^{2+}]_i$ when compared with the concentration without external stimulation. The stationary value of $[Ca^{2+}]_i$ was independent of the maximal pump currents.

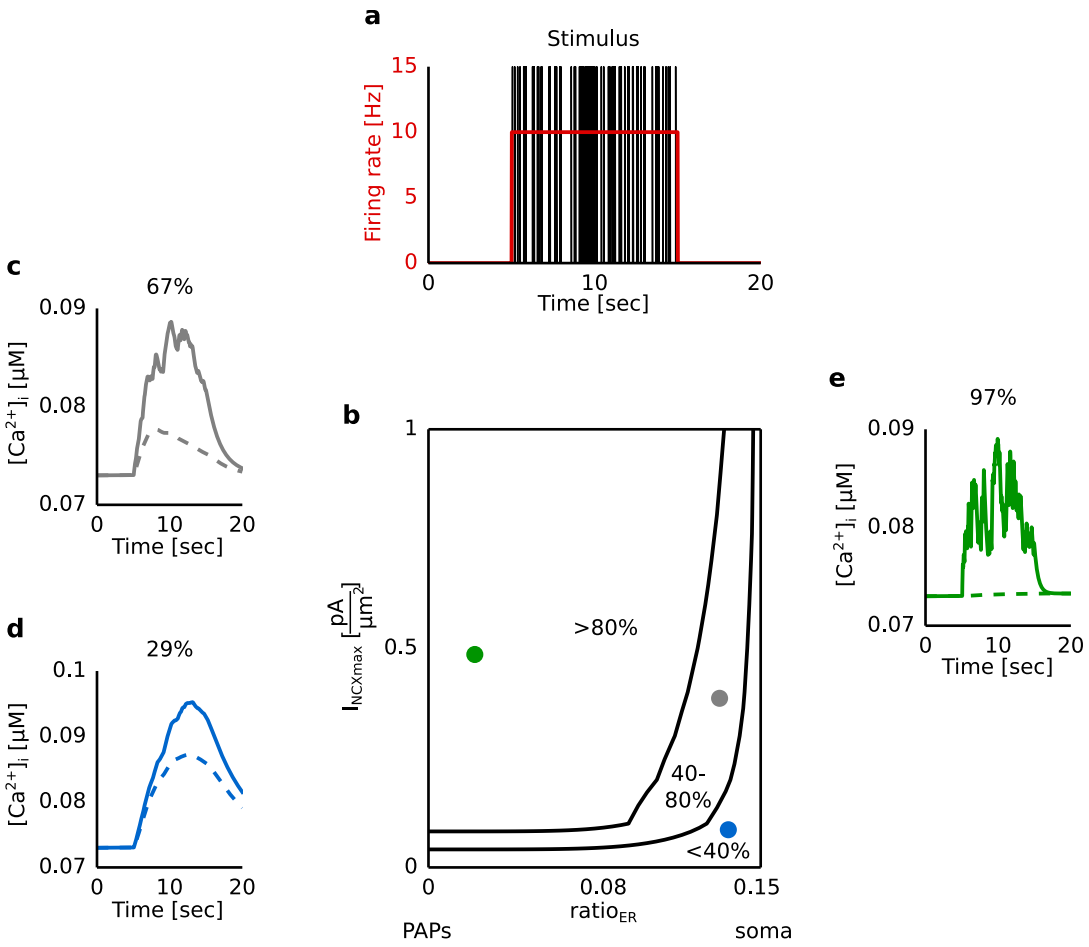

Fig 8. Dynamics of the Ca^{2+} concentration in the intracellular compartment under synaptic stimulation for a blocked glutamate transporter (GluT) in comparison to the control condition. a The astrocytic compartment was stimulated for 10 seconds with a Poisson spike train of 10 Hz. The corresponding glutamate concentration in the extracellular compartment as a function of time was calculated using the Tsodyks and Markram model. **b** Reduction of the Ca^{2+} response under block of the GluT as a function of the maximal pump current of the Na^+/Ca^{2+} exchanger (I_{NCXmax}) and the volume ratio ($ratio_{ER}$) between the internal Ca^{2+} store and the intracellular compartment. The reduction was quantified by the difference of the average Ca^{2+} concentration under control condition and block normalized by the difference between the Ca^{2+} concentration in the control condition and the Ca^{2+} concentration without stimulation. Solid lines separate the parameter space concerning the reduction: larger than 80%, between 40% and 80% and under 40%. **c-e** Ca^{2+} response as a function of time for different values of I_{NCXmax} and $ratio_{ER}$ correspond to a reduction of the Ca^{2+} signal of 29%, 67% and 97%. Solid and dashed lines correspond to control condition and block. The block was simulated by setting $I_{GluTmax}$ equal to 0 $\frac{pA}{\mu m^2}$.

doi:10.1371/journal.pcbi.1005377.g008

When both the GluT- and mGluR-dependent pathway were considered (see Fig 9b–9f) a high I_{NCXmax} ($I_{NCX_{max}} > 0.001\frac{pA}{\mu m^2}$) caused an increase of the concentration of IP_3 and the fraction h of open IP_3 receptor channels. This caused Ca^{2+} flux out of the internal Ca^{2+} store leading to a decrease of $[Ca^{2+}]_{ER}$ compared to the resting concentration. The concentration of Ca^{2+} in the intracellular space, however, increased by 0.1 μM while $[Ca^{2+}]_o$ increased by 3 μM compared to its resting concentration. For high values of the maximal pump current of the Na^+/Ca^{2+} exchanger the Ca^{2+} transport into the endoplasmatic reticulum mediated by the SERCA pump was overcompensated by the highly strong outflux of Ca^{2+} via the Na^+/Ca^{2+} exchanger (see **S??**). Thus, Ca^{2+} accumulated in the extracellular space, which prevented the generation of Ca^{2+} oscillations.

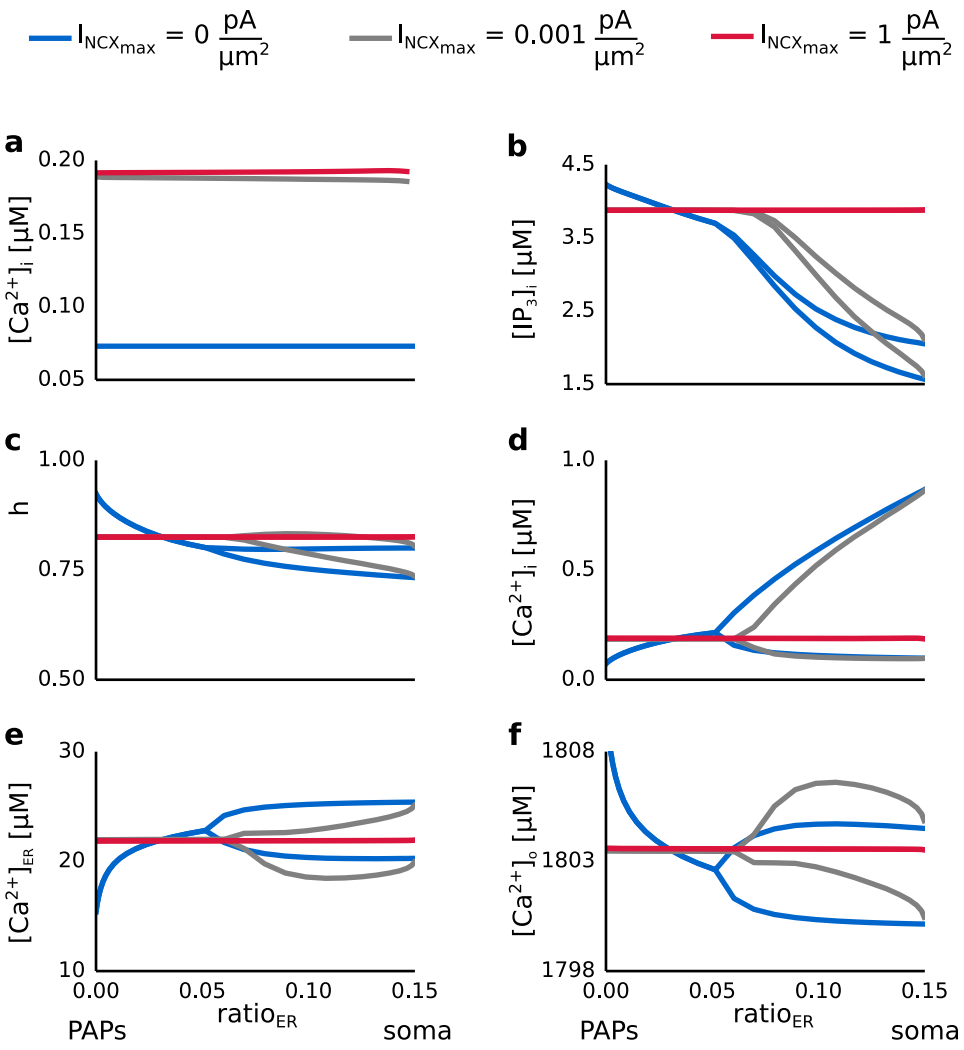

Fig 9. Ca^{2+} concentrations in the intracellular space, the internal Ca^{2+} store and the extracellular space, the IP_3 concentration in the intracellular space and the ratio h of active IP_3 receptor channels as a function of the maximal pump current of the Na^+/Ca^{2+} exchanger (I_{NCXmax}) and the volume ratio between the internal Ca^{2+} store and the intracellular space ($ratio_{ER}$). The astrocytic compartment was stimulated for 200 seconds with a Poisson spike train of 100 Hz. The corresponding glutamate concentration in the extracellular compartment as a function of time was calculated using the Tsodyks and Markram model. Blue, gray and red lines denote the dynamics of $[IP_3]_i$, h $[Ca^{2+}]_i$, $[Ca^{2+}]_{ER}$, $[Ca^{2+}]_o$ for values of I_{NCXmax} equal to 0 $\frac{pA}{\mu m^2}$, 0.001 $\frac{pA}{\mu m^2}$ and 1 $\frac{pA}{\mu m^2}$. **a** Analysis of the GluT-dependent pathway in isolation. $[Ca^{2+}]_i$ is shown as a function of $ratio_{ER}$ and for different values of I_{NCXmax}. **b-f** Analysis of both the mGluR- and the GluT-dependent pathway. $[IP_3]_i$, h, $[Ca^{2+}]_i$, $[Ca^{2+}]_{ER}$ and $[Ca^{2+}]_o$ are shown as a function of $ratio_{ER}$ and for different values of I_{NCXmax}.

doi:10.1371/journal.pcbi.1005377.g009

Discussion

Our computational study addresses the generation of Ca^{2+} signals in different astrocytic compartments along the astrocytic process. We considered two different pathways for the generation of Ca^{2+} signals: the metabotropic glutamate receptor (mGluR)- and glutamate transporter (GluT)-dependent pathway. We analyzed both pathways in consideration of the volume ratio between the internal Ca^{2+} store and the intracellular space. The volume ratio between the internal Ca^{2+} store and the intracellular space changes from the soma towards the synapse. Whereas astrocytic compartments at the soma have a high volume ratio between the internal

Ca^{2+} store and the intracellular space, in astrocytic compartments close to the synapse there is a low volume ratio. There are five main findings of the study.

First, while considering the mGluR-dependent pathway in isolation Ca^{2+} oscillations have only been observed in astrocytic compartments with a high volume ratio between the internal Ca^{2+} store and the intracellular space. Second, a high maximal pump current of the Na^+/Ca^{2+} exchanger suppressed Ca^{2+} oscillations in regions with a high volume ratio between the internal Ca^{2+} store and the intracellular space. Third, the suppression of Ca^{2+} oscillations for a high maximal pump current of the Na^+/Ca^{2+} exchanger in astrocytic compartments with a high volume ratio between the internal Ca^{2+} store and the intracellular space was due to an overcompensation of the Ca^{2+} influx from the internal Ca^{2+} store by the outflux of Ca^{2+} into the extracellular space via the Na^+/Ca^{2+} exchanger. Fourth, a high impact of the GluT-dependent mechanism on the generation of Ca^{2+} signals was observed for a high maximal pump current of the Na^+/Ca^{2+} exchanger in regions with a low volume ratio between the internal Ca^{2+} store and the intracellular space. Fifth, the GluT-dependent mechanism accounted for Ca^{2+} fluctuations in astrocytic compartments which were devoid of internal Ca^{2+} stores.

In their study Srinivasan and colleagues also addressed the question which mechanism could account for Ca^{2+} fluctuations in astrocytic compartments close to the synapse. They discovered that a significant proportion of Ca^{2+} signals in astrocytic compartments close to the synapse is because of transmembrane Ca^{2+} fluxes. In our model we also considered Ca^{2+} transport from the extracellular space into the intracellular space of the astrocyte through the GluT-dependent pathway. We found that the GluT-dependent Ca^{2+} transport into the astrocyte could account for mGluR-independent Ca^{2+} fluctuations in astrocytic compartments with a low volume ratio between the internal Ca^{2+} store and the intracellular space.

However, while analyzing both the mGluR- and GluT-dependent pathway a high maximal pump current of the Na^+/Ca^{2+} exchanger suppressed Ca^{2+} oscillations in astrocytic compartments with a high volume ratio between the internal Ca^{2+} store and the intracellular space. Moreover, the contribution of the GluT on the generation of Ca^{2+} signals was highest for a large maximal pump current of the Na^+/Ca^{2+} exchanger in astrocytic compartments with a low volume ratio between the internal Ca^{2+} store and the intracellular space. These simulation results suggested a change of the pumping activity of the Na^+/Ca^{2+} exchanger along the astrocytic process. A low maximal pump current in astrocytic compartments at the soma prevented the suppression of Ca^{2+} oscillations. A high maximal pump current in astrocytic compartments close to the synapse allowed a high contribution of the GluT-dependent pathway on the generation of Ca^{2+} signals. Based on the strength of the maximal pump current the channel density of the Na^+/Ca^{2+} exchanger can be concluded. The higher the maximal pump current is, the more ions are transported through the membrane. The same holds true for the channel density. The higher the channel density is, the more ions are transported through that channel. Experimental results confirm a concentration and colocalization of Na^+/Ca^{2+} exchangers, Na^+/K^+-ATPases and GluTs in perisynaptic astrocytic processes [31, 32].

Ca^{2+} transport through the plasma membrane (e.g. via the Na^+/Ca^{2+} exchanger) [23, 33, 34] as well as by the Ca^{2+} diffusion within a single astrocyte [35, 36] or between astrocytes [37] changes the intracellular Ca^{2+} concentration. Fluctuations of the intracellular Ca^{2+} concentration affect both the Ca^{2+} entry mediated by the Na^+/Ca^{2+} exchanger when operating in the reverse mode [23] and the Ca^{2+} release probability of the endoplasmatic reticulum [38]. The current model neglects Ca^{2+} diffusion within the astrocyte and describes the Ca^{2+} dynamics in a single compartment. Thus, an extension of the current point-model to a multi-compartment model will most probably reveal deviating results for parameters such as the maximal pump current of the Na^+/Ca^{2+} exchanger. Moreover, the volume determines the number of Ca^{2+} ions within an astrocytic compartment and consequently the concentration change. Thus,

diffusion of Ca^{2+} in astrocytic compartments with a low volume, such as in the perisynaptic astrocytic processes, leads to a bigger concentration change as in compartments with a larger volume.

The above named findings allow to make a prediction about the functional role of astrocytes in neural networks. Astrocytic compartments, which have a high volume ratio of internal Ca^{2+} stores and are capable of IP_3-dependent Ca^{2+} release, are not located directly at the synapse. Moreover, the high surface volume ratio of the perisynaptic astrocytic processes and a slow diffusion exchange in such thin processes favors a localized Na^+ accumulation and promotes Ca^{2+} intrusion mediated by the NCX [39]. This may indicate that store-dependent Ca^{2+} signals in astrocytes act as integrators of local network activity, but not as detectors of individual synaptic events [12]. GluT-dependent Ca^{2+} signals in perisynaptic astrocytic processes are evoked in response to individual synaptic events. Depending on the synaptic activity Ca^{2+} is transported into the astrocyte by the Na^+/Ca^{2+} exchanger and diffuses within the astrocyte network. Once this Ca^{2+} wave reaches astrocytic compartments which are capable of store dependent Ca^{2+} signals an integration of the local network activity, the intracellular Ca^{2+} signal and the glutamate-dependent IP_3 production, takes place.

Our model describes the generation of Ca^{2+} signals in a single astrocyte compartment with respect to its morphology. However, it is of special interest how activity of single synapses and neural networks is integrated by astrocytes. It was proposed that perisynaptic astrocytic processes serve as detectors for single synaptic events, whereas astrocytic processes which contain Ca^{2+} stores act as integrators of neural network activity [12]. A multi-compartment model would contribute to the analysis of the integration of neural activity performed by astrocytes. This would allow the study of Ca^{2+} waves within a single astrocyte and in astrocyte networks as well as their impact on the surrounding extracellular space.

Supporting information

S1 Fig. Increase of the intracellular Na^+ concentration during synaptic stimulation. Dynamics of the Na^+ concentration in the intracellular compartment under synaptic stimulation for a blocked glutamate transporter in comparison to the control condition. The astrocytic compartment was stimulated for 10 seconds with a Poisson spike train of 10 Hz (see Fig 8). **a** Time course of the glutamate concentration in the extracellular compartment calculated with the Tsodyks and Markram model. **b-d** Time course of the intracellular Na^+ concentration for three different parameter combinations of the volume ratio between the internal Ca^{2+} store and the intracellular space ($ratio_{ER}$) and the maximal pump current of the Na^+/Ca^{2+} exchanger ($I_{NCX_{max}}$). The intracellular Na+ concentration is shown for the same parameter combinations of $I_{NCX_{max}}$ and $ratio_{ER}$ as Ca^{2+} in Fig 8c, 8d and 8e (**b**: $ratio_{ER} = 0.14$ and $I_{NCX_{max}} = 0.1 \frac{pA}{\mu m^2}$, **c**: $ratio_{ER} = 0.12$ and $I_{NCX_{max}} = 0.4 \frac{pA}{\mu m^2}$, **d**: $ratio_{ER} = 0.03$ and $I_{NCX_{max}} = 0.5 \frac{pA}{\mu m^2}$). Solid and dashed lines corresponds to the control condition and block, respectively. The intracellular Na^+ concentration was not affected by different values of $ratio_{ER}$ and $I_{NCX_{max}}$. During a block of the glutamate transporter (dashed lines) the Na^+ concentration remained on its resting concentration.
(EPS)

S2 Fig. Impact of the stimulation frequency on the Ca^{2+} oscillation frequency. Ca^{2+} oscillation frequency as a function of the maximal pump current of the Na^+/Ca^{2+} exchanger ($I_{NCX_{max}}$) and the stimulation frequency, as well as for different values of the volume fraction of the internal Ca^{2+} store ($ratio_{ER}$). The astrocytic compartment was stimulated for 200 seconds with a

Poisson spike train of 5-100 Hz. The corresponding glutamate concentration was calculated using the Tsodyks Markram model. The parameter space for which Ca^{2+} oscillations were observed increased with an increase of $ratio_{ER}$. An onset of the Ca^{2+} oscillations was observed for stimulation frequencies greater than 5 Hz. The oscillation frequency, however, decreased for an increase of the volume fraction of internal Ca^{2+} stores. Thus, a larger volume of the internal Ca^{2+} store and the intracellular space favored the generation of Ca^{2+} oscillations and a longer Ca^{2+} oscillation period.
(EPS)

S3 Fig. Impact of the stimulation frequency on the current strength of the Na^+/Ca^{2+} exchanger. Current strength of the Na^+/Ca^{2+} exchanger (I_{NCX}) as a function of the maximal pump current of the Na^+/Ca^{2+} exchanger ($I_{NCX_{max}}$) and the stimulation frequency, as well as for different values of the volume fraction of the internal Ca^{2+} store ($ratio_{ER}$). The astrocytic compartment was stimulated for 200 seconds with a Poisson spike train of 5-100 Hz. The corresponding glutamate concentration was calculated using the Tsodyks Markram model. The white area corresponds to parameter combinations which evoked Ca^{2+} oscillations. An increase of the volume fraction of the internal Ca^{2+} store led to a decrease of I_{NCX}, which corresponded to a larger outflux of Ca^{2+} out of the astrocyte.
(EPS)

S4 Fig. Response of the model to a single action potential. Time course of the intracellular Ca^{2+} concentration, the current strengths of the Na^+/Ca^{2+} exchanger and the IP_3-receptor current for different values of the maximal pump current of the Na^+/Ca^{2+} exchanger ($I_{NCX_{max}}$) and the volume fraction of the internal Ca^{2+} store ($ratio_{ER}$). **a** The astrocytic compartment was stimulated with a single action potential. The gray line corresponds to the time point of the action potential. The corresponding glutamate concentration was calculated using the Tsodyks Markram model. **b-d** Time courses of the intracellular Ca^{2+} concentration $[Ca^{2+}]_i$, the current strengths of the Na^+/Ca^{2+} (I_{NCX}) and the IP_3-receptor current (I_{IP_3R}) for different values of $I_{NCX_{max}}$ and $ratio_{ER}$. After the application of a single action potential the Ca^{2+} concentration returned fastest to the resting concentration when the astrocytic compartment was devoid of the internal Ca^{2+} store ($ratio_{ER} = 0$) (see **b**). This process was slowed down by the Ca^{2+} transport mechanisms at the internal Ca^{2+} store ($ratio_{ER} = 0.06$ and 0.15). In general, the current strength of the Na^+/Ca^{2+} exchanger reached the steady state much faster than the current strength of the IP_3-receptor current (see **c, d**). With an increase of the volume fraction of the internal Ca^{2+} store also the impact of the Ca^{2+} transport mechanisms at the endoplasmatic reticulum on the intracellular Ca^{2+} concentration increased. Thus, for larger values of $ratio_{ER}$ it took longer for Ca^{2+} to return to its resting concentration.
(EPS)

Author Contributions

Conceptualization: FO KM EJ KO.

Funding acquisition: FO KM KO.

Investigation: FO KM EJ.

Methodology: FO KM EJ KO.

Software: FO KM EJ.

Writing – original draft: FO KO.

References

1. Perea G, Navarrete M, Araque A. Tripartite synapses: astrocytes process and control synaptic information; 2009.
2. Helen C, Kastritsis C, Salm AK, McCarthy K. Stimulation of the P2Y Purinergic Receptor on Type 1 Astroglia Results in Inositol Phosphate Formation and Calcium Mobilization. Journal of Neurochemistry. 1992; 58(4):1277–1284. doi: 10.1111/j.1471-4159.1992.tb11339.x
3. McCarthy KD, Salm AK. Pharmacologically-distinct subsets of astroglia can be identified by their calcium response to neuroligands. Neuroscience. 1991; 41(2-3):325–333. doi: 10.1016/0306-4522(91)90330-Q PMID: 1678498
4. Pasti L, Volterra A, Pozzan T, Carmignoto G. Intracellular calcium oscillations in astrocytes: a highly plastic, bidirectional form of communication between neurons and astrocytes in situ. The Journal of neuroscience: the official journal of the Society for Neuroscience. 1997; 17(20):7817–30.
5. Araque A, Martín ED, Perea G, Arellano JI, Buño W. Synaptically released acetylcholine evokes Ca2+ elevations in astrocytes in hippocampal slices. The Journal of neuroscience: the official journal of the Society for Neuroscience. 2002; 22(7):2443–50.
6. Agulhon C, Petravicz J, McMullen AB, Sweger EJ, Minton SK, Taves SR, et al. What is the role of astrocyte calcium in neurophysiology? Neuron. 2008; 59(6):932–946. doi: 10.1016/j.neuron.2008.09.004 PMID: 18817732
7. Wallach G, Lallouette J, Herzog N, De Pittà M, Jacob EB, Berry H, et al. Glutamate Mediated Astrocytic Filtering of Neuronal Activity. PLoS Computational Biology. 2014; 10(12). doi: 10.1371/journal.pcbi.1003964 PMID: 25521344
8. Schummers J, Yu H, Sur M. Tuned responses of astrocytes and their influence on hemodynamic signals in the visual cortex. Science (New York, NY). 2008; 320(5883):1638–43. doi: 10.1126/science.1156120
9. Rojas H, Colina C, Ramos M, Benaim G, Jaffe EH, Caputo C, et al. Na+ entry via glutamate transporter activates the reverse Na+/Ca2+ exchange and triggers Cai 2+ -induced Ca2+ release in rat cerebellar Type-1 astrocytes. Journal of Neurochemistry. 2007; 100(5):1188–1202. doi: 10.1111/j.1471-4159.2006.04303.x PMID: 17316398
10. Rose EM, Koo JCP, Antflick JE, Ahmed SM, Angers S, Hampson DR. Glutamate Transporter Coupling to Na,K-ATPase. Journal of Neuroscience. 2009; 29(25):8143–8155. doi: 10.1523/JNEUROSCI.1081-09.2009 PMID: 19553454
11. Srinivasan R, Huang BS, Venugopal S, Johnston AD, Chai H, Zeng H, et al. Ca(2+) signaling in astrocytes from Ip3r2(-/-) mice in brain slices and during startle responses in vivo. Nature neuroscience. 2015; 18(5):708–17. doi: 10.1038/nn.4001 PMID: 25894291
12. Patrushev I, Gavrilov N, Turlapov V, Semyanov A. Subcellular location of astrocytic calcium stores favors extrasynaptic neuron-astrocyte communication. Cell Calcium. 2013; 54(5):343–349. doi: 10.1016/j.ceca.2013.08.003 PMID: 24035346
13. De Pittà M, Goldberg M, Volman V, Berry H, Ben-Jacob E. Glutamate regulation of calcium and IP3 oscillating and pulsating dynamics in astrocytes. Journal of Biological Physics. 2009; 35(4):383–411. doi: 10.1007/s10867-009-9155-y PMID: 19669422
14. Li YX, Rinzel J. Equations for InsP3 Receptor-mediated [Ca2+]i Oscillations Derived from a Detailed Kinetic Model: A Hodgkin-Huxley Like Formalism. Journal of Theoretical Biology. 1994; 166(4):461–473. doi: 10.1006/jtbi.1994.1041 PMID: 8176949
15. Tzingounis AV, Wadiche JI. Glutamate transporters: confining runaway excitation by shaping synaptic transmission. Nat Rev Neurosci. 2007; 8(12):935–947. doi: 10.1038/nrn2274 PMID: 17987031
16. Kanner BI, Bendahan A. Binding order of substrates to the sodium and potassium ion coupled L-glutamic acid transporter from rat brain. Biochemistry. 1982; 21(24):6327–6330. doi: 10.1021/bi00267a044 PMID: 6129891
17. Wadiche JI, Arriza JL, Amara SG, Kavanaugh MP. Kinetics of a human glutamate transporter. Neuron. 1995; 14(5):1019–1027. doi: 10.1016/0896-6273(95)90340-2 PMID: 7748550
18. Luo C. A dynamic model of the cardiac ventricular action potential. I. Simulations of ionic currents and concentration changes. Circulation Research. 1994; 74(6). doi: 10.1161/01.RES.74.6.1097 PMID: 7514509
19. Østby I, Øyehaug L, Einevoll GT, Nagelhus EA, Plahte E, Zeuthen T, et al. Astrocytic mechanisms explaining neural-activity-induced shrinkage of extraneuronal space. PLoS Computational Biology. 2009; 5(1):e1000272. doi: 10.1371/journal.pcbi.1000272 PMID: 19165313
20. Blaustein MP, Santiago EM. EFFECTS OF INTERNAL AND EXTERNAL CATIONS AND OF ATP ON SODIUM-CALCIUM AND CALCIUM-CALCIUM EXCHANGE IN SQUID AXONS with the technical assistance of. Biophys J. 1977; 20(1):79–111.

21. Tsodyks MV, Markram H. The neural code between neocortical pyramidal neurons depends on neurotransmitter release probability. Proceedings of the National Academy of Sciences. 1997; 94(2):719–723. doi: 10.1073/pnas.94.2.719

22. Fuhrmann G, Markram H, Tsodyks M. Spike frequency adaptation and neocortical rhythms. J Neurophysiol. 2002; 88(2):761–770. PMID: 12163528

23. Reyes RC, Verkhratsky A, Parpura V. Plasmalemmal Na+/Ca2+ exchanger modulates Ca2+-dependent exocytotic release of glutamate from rat cortical astrocytes. ASN neuro. 2012; 4(1):33–45. doi: 10.1042/AN20110059 PMID: 22268447

24. McKhann GM, D'Ambrosio R, Janigro D. Heterogeneity of astrocyte resting membrane potentials and intercellular coupling revealed by whole-cell and gramicidin-perforated patch recordings from cultured neocortical and hippocampal slice astrocytes. The Journal of neuroscience: the official journal of the Society for Neuroscience. 1997; 17(18):6850–63.

25. Falcke M, Hudson JL, Camacho P, Lechleiter JD. Impact of Mitochondrial Ca2+ Cycling on Pattern Formation and Stability. Biophysical Journal. 1999; 77(1):37–44. doi: 10.1016/S0006-3495(99)76870-0 PMID: 10388738

26. Ullah G, Jung P, Cornell-Bell AH. Anti-phase calcium oscillations in astrocytes via inositol (1, 4, 5)-trisphosphate regeneration. Cell Calcium. 2006; 39(3):197–208. doi: 10.1016/j.ceca.2005.10.009 PMID: 16330095

27. Horak FB, Nashner LM, Diener HC. Characterization of glutamate uptake into and release from astrocytes and neurons cultured from different brain regions. Experimental Brain Research. 1990; 47 (2):167–177.

28. Goodman D, Brette R. Brian: a simulator for spiking neural networks in python. Frontiers in neuroinformatics. 2008; 2(November):5. doi: 10.3389/neuro.11.005.2008 PMID: 19115011

29. Kirischuk S, Kettenmann H, Verkhratsky A. Membrane currents and cytoplasmic sodium transients generated by glutamate transport in Bergmann glial cells. Pflügers Archiv—European Journal of Physiology. 2007; 454(2):245–252. doi: 10.1007/s00424-007-0207-5 PMID: 17273865

30. Rose CR, Karus C. Two sides of the same coin: Sodium homeostasis and signaling in astrocytes under physiological and pathophysiological conditions. Glia. 2013; 61(8):1191–1205. doi: 10.1002/glia.22492 PMID: 23553639

31. Minelli A, Castaldo P, Gobbi P, Salucci S, Magi S, Amoroso S. Cellular and subcellular localization of Na+-Ca2+ exchanger protein isoforms, NCX1, NCX2, and NCX3 in cerebral cortex and hippocampus of adult rat. Cell Calcium. 2007; 41(3):221–234. doi: 10.1016/j.ceca.2006.06.004 PMID: 16914199

32. Danbolt NC. Glutamate uptake; 2001. Available from: http://www.ncbi.nlm.nih.gov/pubmed/11369436.

33. Goldman WF, Yarowsky PJ, Juhaszova M, Krueger BK BM. Sodium/calcium exchange in rat cortical astrocytes. J Neurosci. 1994; 14(14):5834–5843. PMID: 7523629

34. Kirischuk S, Ketfenmann H. Na+/ Ca2+exchanger modulates Ca2+ signaling in Bergmann glial cells in situ. Federation of American Societies for Experimental Biology. 1997; 11(7):566–572.

35. Grosche J, Matyash V, Möller T, Verkhratsky A, Reichenbach A, Kettenmann H. Microdomains for neuron-glia interaction: parallel fiber signaling to Bergmann glial cells. Nature neuroscience. 1999; 2 (2):139–43. doi: 10.1038/5692 PMID: 10195197

36. Kirischuk S, Moller T, Voitenko N, Kettenmann H, Verkhratsky A. ATP-induced cytoplasmic calcium mobilization in Bergmann glial cells. Journal of Neuroscience. 1995; 15(12). PMID: 8613725

37. Cornell-Bell AH, Finkbeiner SM, Cooper MS, Smith SJ. Glutamate induces calcium waves in cultured astrocytes: long- range glial signalling. Science. 1990; 247(4941):470–473. doi: 10.1126/science.1967852 PMID: 1967852

38. Bezprozvanny I, Watras J, Ehrlich BE. Bell-shaped calcium-response curves of Ins(1,4,5)P3- and calcium-gated channels from endoplasmic reticulum of cerebellum.; 1991. Available from: http://www.ncbi.nlm.nih.gov/pubmed/1648178 http://dx.doi.org/10.1038/351751a0.

39. Rusakov DA, Zheng K, Henneberger C. Astrocytes as Regulators of Synaptic Function A Quest for the Ca2+ Master Key. The Neuroscientist. 2011; 17(5):513–523. doi: 10.1177/1073858410387304 PMID: 21536839